Progress In Electromagnetics Research B, Vol. 9, 263–279, 2008

ANALYTICAL FORMULAE FOR RADAR CROSS SECTION OF FLAT PLATES IN NEAR FIELD AND NORMAL INCIDENCE

P. Pouliguen and R. Hemon †

Centre d'Electronique de l'Armement
Division CGN
35170 Bruz, France

C. Bourlier

IREENA
Polytech'Nantes
La Chantrerie, rue C. Pauc, 44306 Nantes cedex 3, France

J. F. Damiens

Centre d'Electronique de l'Armement
Division CGN
35170 Bruz, France

J. Saillard

IREENA
Polytech'Nantes
La Chantrerie, rue C. Pauc, 44306 Nantes cedex 3, France

Abstract—Radar Cross Section is most of the time defined in far field. In that case, RCS is totally independent of the range between the radar and the target. However, in several kinds of military scenario, it can be more realistic to deal with the target near-field scattering characteristics. Using a relation to define near-field RCS, this communication proposes simple and approximated analytical formulas to express monostatic near-field RCS of perfectly conducting flat targets observed in normal incidence.

† Also with IREENA, Polytech'Nantes, La Chantrerie, rue C. Pauc, 44306 Nantes cedex 3, France.

1. INTRODUCTION

In many operational military scenarios, it can be very useful to deal with the near-field scattering characteristics of the targets. For example, in naval electronic warfare, battleships are most of the times observed in the near-field zone of seekers. Below the Fraunhofer limit, RCS depends on the range between the target and the radar and needs to be evaluated versus this parameter.

To the authors knowledge, very few works are published on near-field RCS computation. Vogel et al. [1] have proposed a Physical Optics (PO) approximation in the near-field region. The surface of the target is approximated by flat surface patches sized in such a way that for each individual patch the far-field approximation applies. Then, the integration over each meshing element is carried out analytically. The reflection from the entire object is calculated by vectorial summation of all individual elementary reflections. More recently, Legault et al. [2] have implemented such a technique to compute RCS of vessels in realistic configurations. In these both works the near-field RCS is defined as the far-field RCS, simply omitting the limit $R \to \infty$. To simulate the radar returns of an airborne target from mid-course to end-game, the NcPTD and Npatch codes [3, 4] have been developed, based on PO/PTD and shooting and bouncing rays methods. Pouliguen et al. have also proposed method [5, 6] to calculate near-field RCS, based on PO and the division of the target surface in sub-surfaces (triangular meshes), in such a way that all the elementary surfaces are located in the far field of the transmitter and the receiver. Also, a new definition of near-field RCS has been proposed, using the transmitter generator voltage rather than the electric field incident on the target surface. This definition allows considering very naturally the non uniform magnitude and phase of the incident EM field on the target surface.

Moreover, unlike the far-field, no simple analytical formulae exist to calculate near-field RCS of simple shaped targets such as plates, discs. Previous works [6, 7] have focused on particular phenomena appearing on monostatic RCS of perfectly conducting flat circular and square plates, when these targets are observed in near-field and for a normal incidence. These phenomena are the periodic or the pseudo-periodic behaviour of the monostatic RCS versus the frequency and also that their maximum values, at a given range as the frequency varies, are only dependant of the observation range and always appear in near-field. This paper proposes simple and approximated analytical formulae to express monostatic near-field RCS of perfectly conducting flat plates observed in normal incidence. Thus, some of the phenomena

shown just numerically in [6, 7] are here more rigorously demonstrated.

2. NEAR-FIELD RCS

In the following, we consider an isotropic antenna radiation in order to focus only on the spherical wave effects. In near-field, the exact expression of RCS (1) relates the electric and magnetic fields scattered by the target $\left\{\vec{E}_s; \vec{H}_s\right\}$ with the electric and magnetic fields incident on the target surface $\left\{\vec{E}_{is}; \vec{H}_{is}\right\}$,

$$\sigma = 4\pi R^2 \frac{\left|\vec{E}_s \wedge \vec{H}_s^*\right|}{\left|\vec{E}_{is} \wedge \vec{H}_{is}^*\right|}. \tag{1}$$

Relation (1) is difficult to apply because it needs to consider the electric and magnetic fields incident on each point of the target surface. So, a first approximation consists in supposing that the EM field radiated by the antenna has a spherical wave structure, locally plane on the target surface, which allows expressing the incident magnetic field in function of the incident electric field. Then, considering the electric field incident on the target in function of the generator voltage V_i (see relation (A9) in appendix A), we obtain the more tractable relation to calculate near-field RCS

$$\sigma \approx 4\pi R^4 Z_0 \frac{\left|\vec{E}_s \wedge \vec{H}_s^*\right|}{|V_i|^2}. \tag{2}$$

In the same way, a second approximation is to consider that the scattered EM wave front has a spherical structure, locally plane on the receiving antenna. In that case, the relation (2) can be also approximated by (3) and (4),

$$\sigma \approx 4\pi R^4 \frac{\left|\vec{E}_s\right|^2}{|V_i|^2}, \tag{3}$$

$$\sigma \approx 4\pi R^4 Z_0^2 \frac{\left|\vec{H}_s\right|^2}{|V_i|^2}. \tag{4}$$

3. ANALYTICAL FORMULAE OF MONOSTATIC NEAR-FIELD RCS OF FLAT PLATES IN NORMAL INCIDENCE

We consider the case of flat plates observed in normal incidence (Radar axis parallel to Z axis), as illustrated on Figure 1. The $e^{-j\omega t}$ time factor has been assumed and suppressed. To demonstrate the remarkable behaviors shown in [6] and [7], we consider the expression of the magnetic field scattered by a perfectly conducting target, obtained from Stratton-Chu integral equation [8] simplified thanks to Physical Optics approximations [9]. Then, applying it to the particular case of a flat surface, we obtain (see appendix A)

$$\vec{H}_s \approx -j\frac{V_i}{\lambda Z_0}\iint_S \left[(\hat{r}\cdot\hat{n})\,\hat{h}_i - \left(\hat{r}\cdot\hat{h}_i\right)\hat{n}\right]\frac{e^{j2kr}}{r^2}dS, \tag{5}$$

with

$$r = \left|\vec{R} - \vec{\rho}\right| = \sqrt{R^2+\rho^2}.$$

In monostatic condition, as $\hat{r}\cdot\hat{h}_i = 0$, Equation (5) becomes:

$$\vec{H}_s \approx -j\frac{V_i}{\lambda Z_0}\iint_S (\hat{r}\cdot\hat{n})\,\hat{h}_i\frac{e^{j2kr}}{r^2}dS. \tag{6}$$

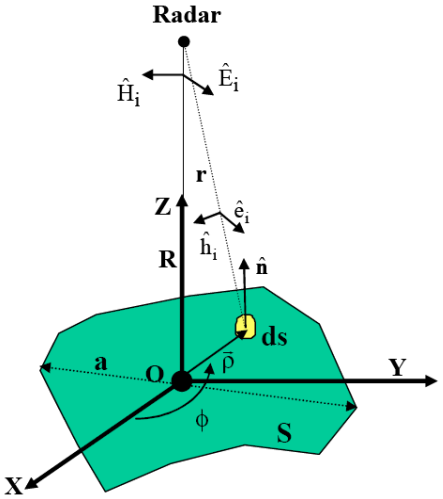

Figure 1. Geometry of the backscattering by a flat plate in near field.

Figure 2 shows the monostatic near-field RCS of a perfectly conducting square plate of side $a = 0.30\,\mathrm{m}$, versus frequency, observed at the range $R = 1\,\mathrm{m}$, calculated using the PO integral (6) in solid line and using the Finite Element Method (FEM) in dashed line. The two methods show a very good correlation, particularly for frequencies superior to 2 GHz, which validates the PO approach. One observes some differences at low frequencies (in and below the resonance region: $F \leq 2\,\mathrm{GHz}$; $a/\lambda \leq 2$) due to the limit of PO validity.

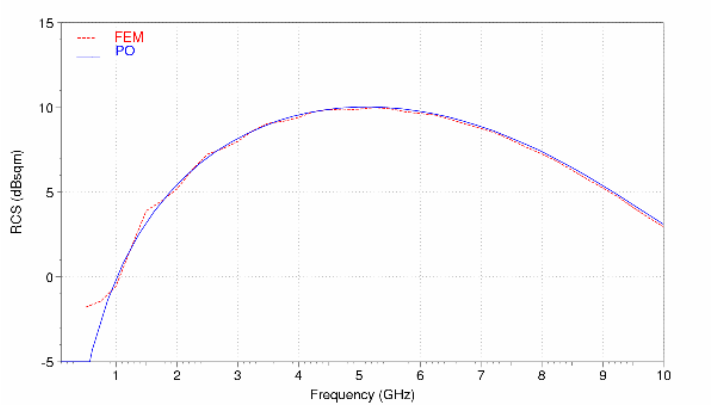

Figure 2. Near-field RCS of a metallic square plate of side 0.30 m versus frequency at $R = 1\,\mathrm{m}$ Comparison between PO (solid line) and FEM (dashed line).

One considers the target size enough small to verify $\rho^2 \ll R^2$ and to allow the following approximations:

$$\text{for the amplitude terms } r \approx R,\ \hat{r}\cdot\hat{n} \approx 1 \text{ and } \hat{h}_i \approx \hat{H}_i, \tag{7a}$$

$$\text{for the phase term } r \approx R + \rho^2/2R \text{ in cylindrical coordinates,} \tag{7b}$$

$$r \approx R + (x^2+y^2)/2R \text{ in Cartesian coordinates.} \tag{7c}$$

These approximations are not a great constraint; for example if $R = 3a$ the minimum value of the quantity $\hat{r}\cdot\hat{n}$ is equal to 0.986 and the maximum value of $r = 3.0414a$ is approximated by $r = 3a$ for the amplitude term and by $r = 3.0417a$ for the phase term.

A. The circular plate case

For the disc of radius a and surface S, considering cylindrical coordinates and substituting approximations (7a) and (7b) in (6), a more compact form is found to describe the backscattered magnetic

field

$$\vec{H}_s \approx -j\frac{2\pi V_i \hat{H}_i e^{j2kR}}{\lambda Z_0 R^2} \int_0^a \rho\, e^{jk\frac{\rho^2}{R}} d\rho. \tag{8}$$

Integrating (8) by parts and using (4) leads to the simple formula of the near-field RCS

$$\sigma \approx 2\pi R^2 \left\{1 - \cos\left(\frac{ka^2}{R}\right)\right\}. \tag{9}$$

This formula confirms the periodic behavior of RCS versus frequency and the empirical formulae established in [6] and [7]. For example (9) shows that the maximum RCS of the disc, at a specified range R as the frequency varies, is equal to

$$\sigma_{\max} \approx 4\pi R^2. \tag{10}$$

Moreover we remark that when R tends toward infinity, relation (9) tends toward the well known formula

$$\sigma \overset{R\to\infty}{\longrightarrow} \frac{4\pi S^2}{\lambda^2}. \tag{11}$$

Figures 3 and 4(a) illustrate the validity of the simple formula (9). On Figure 3(a), the RCS of a perfectly conducting disc of radius $a = 0.30\,\text{m}$ is plotted versus range R at 15 GHz, calculated using the PO integral and also the analytical formula (9). On Figure 3(b), the RCS of the same target is plotted versus frequency at $R = 5\,\text{m}$ and at $R = 10000\,\text{m}$, calculated with the PO integral and (9). We note a good accuracy of the RCS calculated using the analytical formula (9), versus range and frequency, except a slight shift due to the approximations (7).

Figure 4(a) is a zoom on the Figure 3(a) between ranges 0.5 m and 3 m. Its analyze confirms a shift versus range and an error on RCS maximum levels, which decrease as the range R increases, according to the approximations (7) done on the amplitude and phase terms in (6). The accuracy becomes quite acceptable as R becomes greater than three times the target diameter $2a$; in that case the shift is lower than 5 percent of the range.

At lower distances, to enhance accuracy, it is necessary to maintain higher order terms in the phase approximation. For example, if we express the distance r in the phase term as the Taylor series expansion:

$$r \approx R + \rho^2/2R - \rho^4/8R^3 + \rho^6/16R^5 - 5\rho^8/128R^7, \tag{12}$$

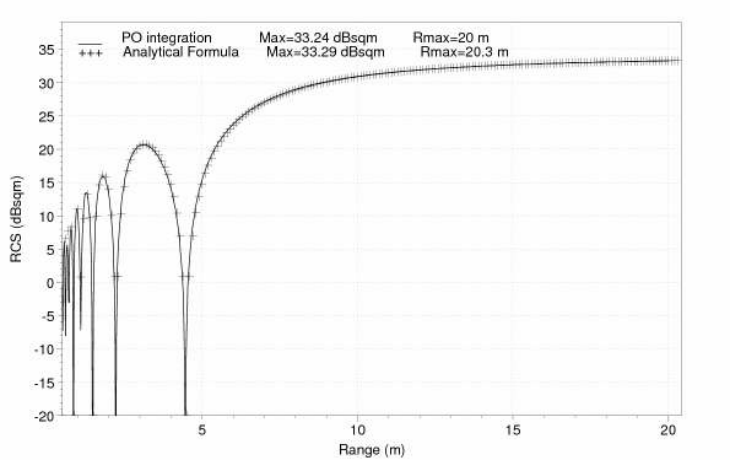

(a)

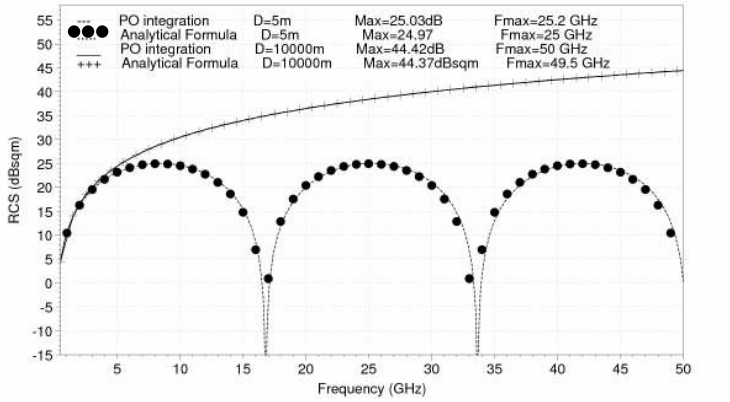

(b)

Figure 3. Monostatic RCS of a disc of radius 0.30 m at normal incidence (a) Above: RCS versus range at $F = 15$ GHz (b) Below: RCS versus frequency at ranges 5 m and 10000 m.

one obtains the following expression of the backscattered magnetic field:

$$\vec{H}_s \approx -j\frac{2\pi V_i \hat{H}_i e^{j2kR}}{\lambda Z_0 R^2} \int_0^a \rho e^{jk\left(\frac{\rho^2}{R} - \frac{\rho^4}{4R^3} + \frac{\rho^6}{8R^5} - \frac{5\rho^8}{64R^7}\right)} d\rho. \tag{13}$$

Then, integrating (13) by parts and using (4), we obtain the following

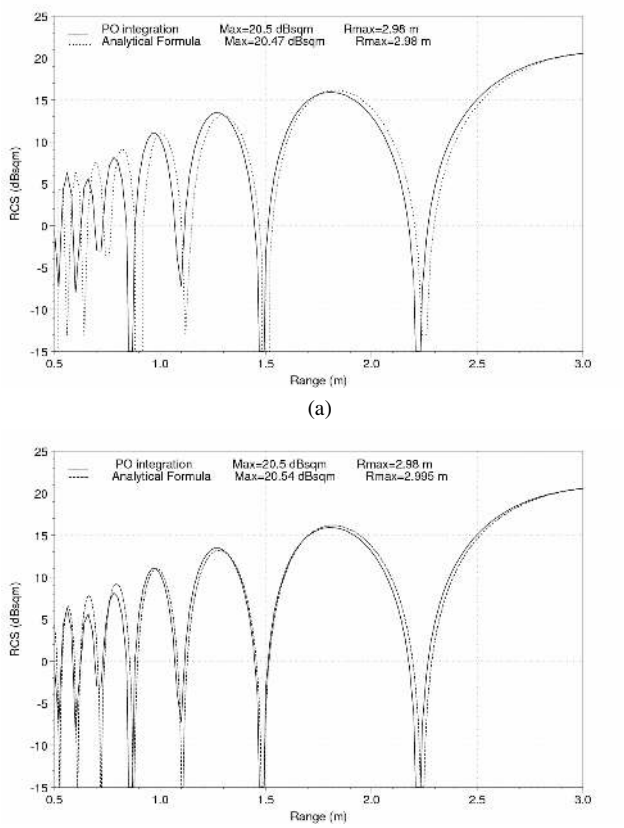

Figure 4. Monostatic RCS of a disc of radius 0.30 m, at normal incidence, zoom versus range at $F = 15\,\mathrm{GHz}$ (a) Above: analytical formula (9) (b) Below: analytical formula (14).

relation for the near-field RCS:

$$\sigma \approx \pi R^2 \left\{ 1 + \frac{1}{\left(1 - \dfrac{a^2}{2R^2} + \dfrac{3a^4}{8R^4} - \dfrac{5a^6}{16R^6}\right)^2} -2\frac{\cos\left(\dfrac{ka^2}{R}\left(1 - \dfrac{a^2}{4R^2} + \dfrac{a^4}{8R^4} - \dfrac{5a^6}{64R^6}\right)\right)}{1 - \dfrac{a^2}{2R^2} + \dfrac{3a^4}{8R^4} - \dfrac{5a^6}{16R^6}} \right\}. \qquad (14)$$

Figure 4(b) shows the same result than given on Figure 4(a), but computed with the formula (14). It confirms that conserving more terms in the phase expansion allows achieving a better accuracy. We particularly observe a significant reduction of the shift which becomes lower than 2.5 percent of the range on the total range domain analyzed.

We also notice that in both cases, formula (9) and (14) describe an identical accuracy on maxima RCS levels. The error on RCS maxima is less than 1 dB as R becomes greater than 1.5 times the target diameter $2a$. To ameliorate this accuracy, it would be convenient to maintain higher order terms also in the amplitude approximations (7).

B. The rectangular plate case

For the rectangular plate of sides a and b, considering Cartesian coordinates and substituting approximations (7a) and (7b) in (6), the backscattered magnetic field is expressed as follows

$$\vec{H}_s \approx -j\frac{V_i\hat{H}_i e^{j2kR}}{\lambda Z_0 R^2}\int\limits_{-a/2}^{a/2} e^{jk\frac{x^2}{R}}dx \int\limits_{-b/2}^{b/2} e^{jk\frac{y^2}{R}}dy. \tag{15}$$

Then, applying the stationary phase method [10] to evaluate these integrals (see appendix B) leads to

$$\vec{H}_s \approx -j\frac{V_i\hat{H}_i e^{j2kR}}{\lambda Z_0 R^2}\left(\sqrt{\frac{R\lambda}{2}}e^{j\frac{\pi}{4}} - j\frac{2R}{ka}e^{j\frac{ka^2}{4R}}\right)\cdot\left(\sqrt{\frac{R\lambda}{2}}e^{j\frac{\pi}{4}} - j\frac{2R}{kb}e^{jk\frac{b^2}{4R}}\right). \tag{16}$$

For the square plate of side a, putting (16) in (4) and developing allow writing the monostatic near-field RCS under the analytical form

$$\sigma \approx 4\pi R^2\left\{\frac{1}{4} + 2X + X^2 - X\sin\left(\frac{1}{\pi X}\right) - \sqrt{2X}\,(1+2X)\sin\left(\frac{\pi}{4} - \frac{1}{2\pi X}\right)\right\}, \tag{17}$$

with

$$X = \frac{R\lambda}{\pi^2 a^2}.$$

This formula confirms the pseudo-periodic behavior of RCS versus frequency and the empirical formulae published in [6] and [7].

In [6], it is shown numerically that the three first maxima of the square plate near-field RCS are:

$$\sigma^1_{\max} \approx \frac{32}{\pi}R^2, \qquad \sigma^2_{\max} \approx 2\pi R^2, \qquad \sigma^3_{\max} \approx \frac{17}{\pi}R^2. \tag{18}$$

In the same way, in [6] it is shown numerically that the three first minima of the square plate near-field RCS are:

$$\sigma^1_{\min} \approx \frac{\pi}{3}R^2, \qquad \sigma^2_{\min} \approx \frac{\pi}{2}R^2, \qquad \sigma^3_{\min} \approx \sqrt{\pi}R^2. \tag{19}$$

We also observe that when the frequency F tends toward infinity and when the range keeps a finite value R, the relation (17) tends toward the following formula:

$$\sigma \overset{F\to\infty}{\longrightarrow} \pi R^2. \tag{20}$$

Figure 5 allows analyzing the validity of the simple formula (17).

Figure 5(a) presents the RCS of a perfectly conducting square plate of side $a = 1\,\text{m}$, versus range R, at 15 GHz, calculated with the PO integral and with the analytical formula (17). Figure 5(b) shows the RCS of the same target versus frequency at $R = 18\,\text{m}$, calculated using the PO integral and using (17), then at $R = 10000\,\text{m}$ (far field) calculated with PO. In both cases, one notes a good accuracy of the analytical formula (17) with the following restrictions:

- When the range becomes important, the RCS calculated with the analytical relation diverges from the PO integration result. Numerical computations show that to obtain RCS accuracy better than 1 dB with (17) it is necessary to verify the criterion:

$$R < 0.0932\frac{\pi^2 a^2}{\lambda}. \tag{21}$$

When the frequency becomes low (below 5GHz), the RCS calculated with the analytical relation diverges also from the PO integration result.

These upper and lower bounds of validity isversus range and frequency are due to the fact that (17) has been established considering only the first term of the asymptotic expansion of the Fresnel integral (B7) which appears when the magnetic field expression (15) is developed using the stationary phase method [10]. This approximation is only valid for large arguments of the Fresnel integral; but when the range becomes large, or when the frequency becomes low, this argument becomes small and it's necessary to keep other terms. Keeping the two first terms of the asymptotic expansion of the Fresnel

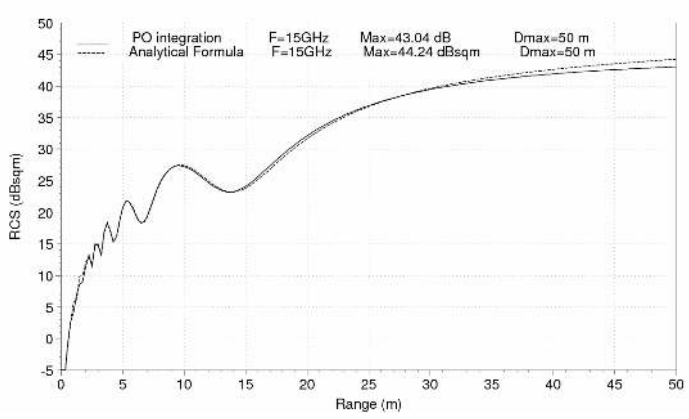

(a)

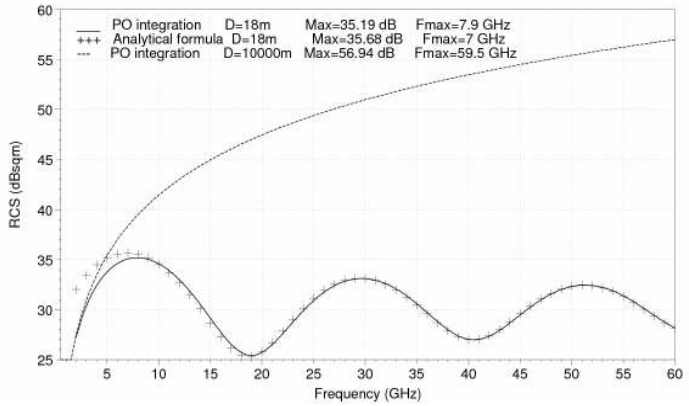

(b)

Figure 5. Monostatic RCS of a square plate of side $a = 1\,\mathrm{m}$ at normal incidence (a) Above: RCS versus range at $F = 15\,\mathrm{GHz}$ (b) Below: RCS versus frequency at ranges 18 m and 10000 m.

integral leads to the following backscattered magnetic field:

$$\vec{H}_s \approx -j\frac{V_i\hat{H}_i e^{j2kR}}{\lambda Z_0 R^2}\left(\sqrt{\frac{R\lambda}{2}}e^{j\frac{\pi}{4}} - j\frac{2R}{ka}e^{j\frac{ka^2}{4R}}\left(1 - j\frac{\lambda R}{\pi a^2}\right)\right) \times \left(\sqrt{\frac{R\lambda}{2}}e^{j\frac{\pi}{4}} - j\frac{2R}{kb}e^{jk\frac{b^2}{4R}}\left(1 - j\frac{\lambda R}{\pi b^2}\right)\right). \quad (22)$$

Then, a more accurate analytical expression for the near field RCS of

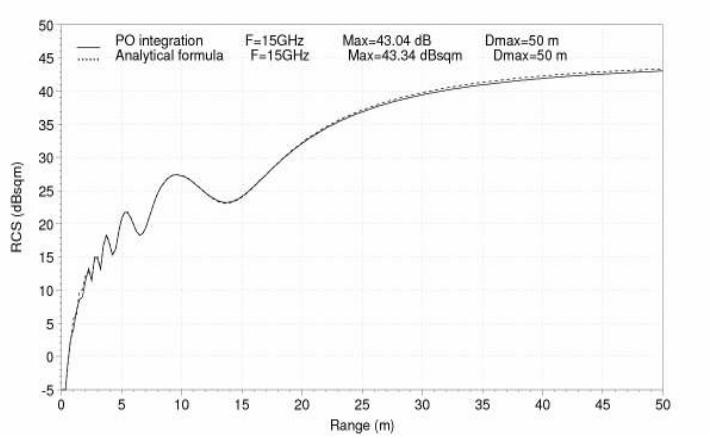

Figure 6a. Monostatic RCS of a square plate of side 1 m at normal incidence, versus range at $F = 15\,\mathrm{GHz}$ — PO integration in solid line — formula (23) in dashed line.

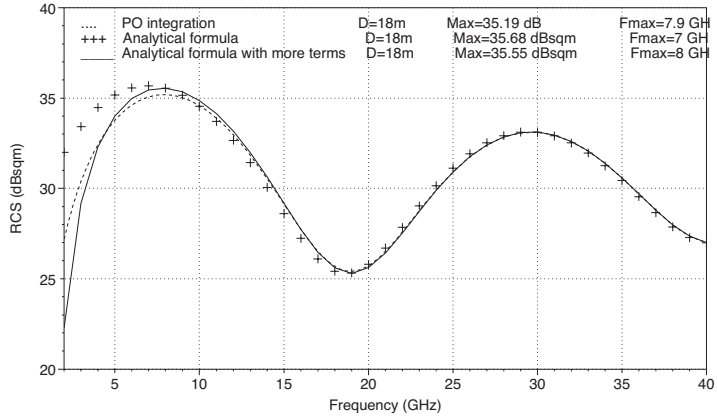

Figure 6b. Monostatic RCS of a square plate of side 1 m at normal incidence versus frequency at 18 m — PO integration in dashed line — formula (17) in cross — formula (23) in solid line.

the rectangular plate is obtained using (22) and (4)

$$\sigma \approx \frac{4\pi}{\lambda^2}\left|\left(\sqrt{\frac{R\lambda}{2}}e^{j\frac{\pi}{4}} - j\frac{2R}{ka}e^{j\frac{ka^2}{4R}}\left(1 - j\frac{\lambda R}{\pi a^2}\right)\right) \times \left(\sqrt{\frac{R\lambda}{2}}e^{j\frac{\pi}{4}} - j\frac{2R}{kb}e^{jk\frac{b^2}{4R}}\left(1 - j\frac{\lambda R}{\pi b^2}\right)\right)\right|^2 \qquad (23)$$

Figure 6a presents the RCS of a perfectly conducting square plate of side $a = b = 1\,\mathrm{m}$ versus range R at 15 GHz, calculated with the PO integral and also with the analytical formula (23). One observes a significant reduction of the error; now the criterion (21) gives RCS accuracy better than 0.3 dB.

- Numerical computations, with (17) and (23), show an error inferior to 1 dB as R becomes greater than three times the target size. This lower bound of validity versus R is mainly due to the phase and amplitude approximations (7). So, it is almost the same for the plate and the disc. Therefore, these results can be enhanced if the amplitude and phase approximations (7) are limited.

4. CONCLUSION

A method based on Physical Optics has been developed to calculate the near-field RCS of targets in the high frequency limit. Then, analytical relations have been established to approximate the monostatic near-field RCS of circular and square flat metallic plates observed in normal incidence. Some validity domains and asymptotic limits are established for these formulae. These new expressions demonstrate the remarkable phenomena already underlined in [6, 7], as the periodic behavior versus frequency of the near-field RCS of a metallic circular plate, and also the dependence of its maximum RCS which is only function of the observation range. Future works will focus on finding such analytical formulae valid in oblique incidence, for flat plates and for other simple shapes. Also we will try to limit some approximations, done on amplitude and phase terms, in order to enhance the accuracy for very low ranges.

APPENDIX A.

The magnetic field scattered by an obstacle of surface S is deduced from the Magnetic field integral equation (MFIE) [8, 9]

$$\vec{H}_s = \frac{1}{4\pi} \iint_S \left(j\omega\varepsilon \vec{M}\phi + \vec{J} \wedge \nabla'\phi + \frac{j}{\omega\mu} \left[\vec{M} \cdot \nabla' \right] \nabla'\phi \right) ds \qquad \text{(A1)}$$

with the $\vec{M} = \vec{E} \wedge \hat{n}$ and $\vec{J} = \hat{n} \wedge \vec{H}$ the magnetic and electric currents induced on S, and with the total EM fields $\vec{E} = \vec{E}_i + \vec{E}_s$ and $\vec{H} = \vec{H}_i + \vec{H}_s$, where $\{\vec{E}_i, \vec{H}_i\}$ and $\{\vec{E}_s, \vec{H}_s\}$ are respectively the incident and scattered EM fields.

$\phi = \frac{e^{jkr}}{r}$ is the Green function and its gradient

$$\nabla'\phi = -\nabla\phi = -\left(jk - \frac{1}{r}\right)\cdot \hat{r} \tag{A2}$$

Using the relation $[\vec{L}\cdot\nabla']\nabla'\phi = \nabla'[\vec{L}\cdot\nabla'\phi]$, one shows that

$$\left[\begin{pmatrix}\vec{J}\\ \vec{M}\end{pmatrix}\cdot\nabla'\right]\nabla'\phi = \left[-(1-jkr)\begin{pmatrix}\vec{J}\\ \vec{M}\end{pmatrix} + (3-j3kr-k^2r^2)\left\{\hat{r}\cdot\begin{pmatrix}\vec{J}\\ \vec{M}\end{pmatrix}\right\}\hat{r}\right]\frac{\phi}{r^2} \tag{A3}$$

Then, replacing (A2) and (A3) in (A1), one obtains

$$\begin{aligned}\vec{H}_s \;=\; & \frac{j}{4\pi\omega\mu}\iint_S \Big[(-1+jkr+k^2r^2)\vec{M} - (k^2r^2+jkr)Z\vec{J}\wedge\hat{r} \\ & + (3-j3kr-k^2r^2)(\hat{r}\cdot\vec{M})\hat{r}\Big]\frac{\phi}{r^2}ds\end{aligned} \tag{A4}$$

Considering the surface S is such that its radii of curvature at all points are much larger than the wavelength [9], it allows approximating it at any point as an infinite plane tangent to the surface at that point. Moreover, if S is perfectly electric conducting, the magnetic and electric currents induced on S are

$$\vec{J} \;=\; 2\hat{n}\wedge\vec{H}_i \tag{A5}$$

$$\vec{M} \;=\; 0 \tag{A6}$$

Putting (A5) and (A6) in (A4) leads to

$$\vec{H}_s \approx \frac{-j}{2\pi\omega\mu}\iint_S \Big[(k^2r^2+jkr)Z_0(\hat{n}\wedge\hat{H}_i)\wedge\hat{r}\Big]\frac{\phi}{r^2}ds \tag{A7}$$

and supposing $kr \gg 1$ allows to write

$$\vec{H}_s \approx \frac{-j}{\lambda}\iint_S \Big[(\vec{n}\wedge\hat{H}_i)\wedge\hat{r}\Big]\phi ds \tag{A8}$$

The incident magnetic field can be expressed

$$\vec{H}_i = \frac{V_i}{Z_0}\frac{e^{jkr}}{r}\hat{h}_i \tag{A9}$$

with V_i the generator voltage.

Finally, substituting (A9) in (A8) and using the vectorial identity $(\hat{a}\wedge\hat{b})\wedge\hat{c} = (\hat{c}\cdot\hat{a})\hat{b} - (\hat{c}\cdot\hat{b})\hat{a}$ lead to

$$\vec{H}_s \approx -j\frac{V_i}{\lambda Z_0}\iint_S \Big[(\hat{r}\cdot\hat{n})\hat{h}_i - (\hat{r}\cdot\hat{h}_i)\hat{n}\Big]\frac{e^{j2kr}}{r^2}ds \tag{A10}$$

APPENDIX B.

We need to solve an integral of the form

$$I = \int_{b_1}^{b_2} f(x) e^{jkg(x)} dx \tag{B1}$$

where $f(x) = 1,\ g(x) = x^2/R,\ b_1 = -a/2$ and $b_2 = a/2$.

The stationary phase approximation [10] allows expressing this integral as

$$I = I_0 - 2I_{a/2} \tag{B2}$$

with

$$I_0 = \sqrt{\frac{2\pi}{k|g''(x_0)|}} f(x_0) \exp\left\{j\left[kg(x_0) + \frac{\pi}{4}\mathrm{sgn}(g''(x_0))\right]\right\} \tag{B3}$$

$$\begin{aligned} I_{a/2} &= U(-\varepsilon) I_0 + \varepsilon f(a/2) \exp\left\{jkg(a/2) \mp jv^2\right\} \\ &\quad \times \sqrt{\frac{2}{k|g''(a/2)|}} F \mp (v) \left\{ g''(\alpha) \begin{matrix} > 0 \\ < 0 \end{matrix} \right\} \end{aligned} \tag{B4}$$

where x_0 is a first order stationary phase point defined by $g'(x_0) = 0$ and $g''(x_0) \neq 0$: Here $x_0 = 0$. $\varepsilon = \mathrm{sgn}(a/2 - x_0)$, $v = \sqrt{\frac{k}{2|g''(a/2)|}} |g'(a/2)|$ and $U(x)$ is the unit step function, i.e., $U = 1$ for $x \geq 0$ and zero otherwise.

$F_{\pm}(x) = \int_x^{\infty} e^{\pm jt^2} dt$ is the Fresnel integral defined for real arguments,

We have $g(x_0) = g'(x_0) = 0,\ g''(x_0) = 2/R,\ g(a/2) = a^2/4R,\ g'(a/2) = a/R,\ g''(a/2) = 2/R,\ v = \sqrt{\frac{ka^2}{4R}}$, which give

$$I_0 = \sqrt{\frac{R\lambda}{2k}} e^{j\frac{\pi}{4}} \tag{B5}$$

$$I_{a/2} = \sqrt{\frac{R}{k}} F \pm \left(\sqrt{\frac{ka^2}{4R}}\right) \tag{B6}$$

For large arguments of the Fresnel integral, its asymptotic expansion is

$$F_{\pm}(x) \approx \frac{1}{2x} \exp\left\{\pm j\left(x^2 + \frac{\pi}{2}\right)\right\} \sum_{m=0}^{\infty} j^{\mp m} \left(\frac{1}{2}\right)_m x^{-2m} \tag{B7}$$

where

$$\left(\frac{1}{2}\right)_0 = 1,\ \left(\frac{1}{2}\right)_m = \frac{1}{2}\left(\frac{1}{2}+1\right)\cdots\left(\frac{1}{2}+m-1\right)$$

Substituting the Fresnel integral by its asymptotic expansion in (B6), we get

$$I_{a/2} = \sqrt{\frac{R}{k}}\left(\frac{1}{2}\sqrt{\frac{4R}{ka^2}}\exp\left\{j\left(\frac{ka^2}{4R}+\frac{\pi}{2}\right)\right\}\sum_{m=0}^{\infty} j^{-m}\left(\frac{1}{2}\right)_m\left(\sqrt{\frac{ka^2}{4R}}\right)^{-2m}\right) \tag{B8}$$

Then, limiting the asymptotic expansion to the first term ($m = 0$) and to the second term ($m = 1$), we find

$$I_{a/2}^{m=0} = j\frac{R}{ka}\exp\left\{j\left(\frac{ka^2}{4R}\right)\right\} \tag{B9a}$$

$$I_{a/2}^{m=1} = j\frac{R}{ka}\exp\left\{j\left(\frac{ka^2}{4R}\right)\right\}\left(1-j\frac{\lambda R}{\pi a^2}\right) \tag{B9b}$$

Combining (B9a) and (B9a) with (B5) and (B2) gives finally

$$I^{m=0} = \sqrt{\frac{R\lambda}{2k}}e^{j\frac{\pi}{4}} - j\frac{2R}{ka}\exp\left\{j\left(\frac{ka^2}{4R}\right)\right\} \tag{B10a}$$

$$I^{m=1} = \sqrt{\frac{R\lambda}{2k}}e^{j\frac{\pi}{4}} - j\frac{2R}{ka}\exp\left\{j\left(\frac{ka^2}{4R}\right)\right\}\left(1-j\frac{\lambda R}{\pi a^2}\right) \tag{B10b}$$

REFERENCES

1. Vogel, M. H., "The physical optics approximation in the near-field region," report no FEL 1989-100n TNO Physics and Electronics Laboratory, March 1989.
2. Legault, S. R. and A. Louie, "Validation and implementation of a near-field Physical Optics formulation," Defence R&D Canada Ottawa, Technical Memorandum, DRDC Ottawa TM 2004-131, August 2004.
3. Yu, C. L., R. Kipp, D. J. Andersh, and S. W. Lee, "Near-field electromagnetic modeling and analysis," *IEEE AP-S International Symposium and URSI Radio Science Meeting*, Montreal, July 13–18, 1997.

4. Lee, S. W. and S. K. Jeng, "NcPTD 1.2 a high frequency near-field RCS computation code based on physical theory of diffraction," DEMACO, Inc., Champaign, IL, June 1991.
5. Pouliguen, P., P. Gadenne, and J. Y. Marty, "Radar reflectivity of a target illuminated by a spherical wave," *Symposium AGARD sur l'analyse de la Signature Radar et de la Vidéoscopie des cibles Militaires*, Ankara Turquie, Octobre 7–10, 1996.
6. Pouliguen, P. and L. Desclos, "A physical optics approach to near-field RCS computations," *Annals of Telecommunications*, Vol. 51, Nos. 5–6, 219–226, May–June 1996.
7. Desclos, L. and P. Pouliguen, "The physical optics applied to discs and square plates in near-fields leads to simple formula," *Microwave and Optical Technology Letters*, Vol. 9, No. 5, 278–283, August 1995.
8. Stratton, J. A., *Electromagnetic Theory*, Mc Graw-Hill Book Company, Inc., New York, 1947.
9. Ruck, G. T., D. E. Barrick, W. D. Stuart, and C. K. Krichbaum, *Radar Cross Section Handbook*, Plenum Press, New York, 1970.
10. James, G. L., *Geometrical Theory of Diffraction for Electromagnetic Waves*, 3rd Edition, Peter Peregrinus Ltd., 1986.
11. Pouliguen, P., R. Hémon, J. Saillard, and J. F. Damiens, "RCS computation in near-field," *Days on Diffraction*, St-Petersburg, May 30–June 2, 2006.